47th AIAA/ASME/ASCE/AHS/ASC Structures, Structural Dynamics, and Materials Confere
1 - 4 May 2006, Newport, Rhode Island

AIAA 2006-1684

MARSIS Antenna Flight Deployment Anomaly and Resolution

Douglas S. Adams*
Jet Propulsion Laboratory, California Institute of Technology, Pasadena, CA 91109

and

Mehran Mobrem†
NGST Astro Aerospace, Carpinteria, CA 93013

This paper summarizes the resolution of an in flight anomaly that occurred during the deployment of the first of three MARSIS antenna booms. Characteristics of this deployment are described, along with a correlation to finite element models and measured spacecraft inertias, which allowed the intermediate state of the boom to be accurately determined. Based on this information, a spacecraft maneuver was performed that warmed the stalled hinge and led to the first boom successfully locking into its designed geometry. The confirmed partially deployed boom shape was then used to develop a thermal model of the stalled hinge both in its initial solar attitude and during the successful spacecraft maneuver. Results from the hinge thermal model and component level testing were evaluated in order to determine the root cause of the anomaly and the probability of its recurrence on subsequent deployments. These conclusions were then utilized in planning mitigating actions that were implemented during the remaining two boom deployments. Final flight data are presented for both dipole booms indicating a correctly deployed and healthy antenna. The monopole boom deployment was detected but the final state of the boom is unknown.

Nomenclature

CTE = coefficient of thermal expansion
ζ = critical damping ratio

I. Introduction

THE Mars Advanced Radar for Subsurface and Ionosphere Sounding (MARSIS) antenna is part of an instrument payload onboard the European Space Agency's (ESA) Mars Express (MEX) spacecraft which launched on June 2, 2003 and entered Mars orbit on December 25, 2003. MARSIS is a long wavelength radar sounder that will be used to perform measurements on the Martian ionosphere and to search for evidence of subsurface water. It is designed to operate at altitudes up to 800 km above the Martian surface for subsurface sounding, up to 1200 km for ionospheric sounding, and is capable of making measurements in 1 MHz wide bands centered at 1.8, 3.0, 4.0, and 5.0 MHz. This flexible design allows MARSIS to search for evidence of water as deep as 5 km below the surface.

The antenna for the MARSIS experiment was developed and built by NGST Astro Aerospace. The antenna is made of three Foldable Flattenable Tubes (FFT)™. A full description of the design is presented in Ref. 1. The FFT is an ultra-lightweight deployable structure that is designed purely for use in a space environment. As such, any significant friction, gravity, or air drag, combined with its large dimensions, renders terrestrial based testing of the FFT intractable. Therefore, the verification process for the FFT deployment relied solely on component level testing and analytical simulations performed using ADAMS software.

The deployment of MARSIS, which was initially scheduled for April 20, 2004, was delayed after the discovery that original analysis had underestimated the deployment dynamics. Over the course of the following year an intense

* Senior Engineer, Spacecraft Structures and Dynamics Group, 4800 Oak Grove Dr., MS: 157-500, Member AIAA.
† Chief Analyst, Engineering, 6384 Via Real, Member AIAA.

testing and analysis effort was undertaken that focused on more accurately quantifying the deployment, validating the ADAMS model, and assessing any risk to the health of the Mars Express spacecraft.

Component testing went beyond the original tests done in order to characterize the post buckling behavior of the hinges and their residual strength capability after multiple buckling events. This was necessary since repeated buckling was anticipated based on the increased dynamics in the updated model. The FFT is not designed to take any significant buckling during the deployment and, if the excess dynamics were known at that time, the MARSIS design would have been modified to reduce its stowed energy. Component test results were incorporated into an updated ADAMS model of the deployment which included an automated damping algorithm to account for the discontinuous boom lengths encountered during the deployment. This model was then exercised in a Monte Carlo study in order to determine the probability of a successful or dangerous deployment outcome. Results obtained from the component tests were ultimately responsible for the successful deployment of the MARSIS booms. For a detailed discussion of the deployment analysis please see the discussion in Refs. 2 and 3.

MARSIS employs a total of three FFT booms with two booms that form a 40 m dipole and the third acting as a 7 m monopole antenna. The booms have periodic slotted hinge sections where some material is removed which then allows the Kevlar and fiberglass composite tubes to be folded elastically without permanent deformation. The folded booms are then compressed accordion style into a cradle for launch and the journey to Mars as shown in Fig. 1. Each boom is thus a single piece structure in its deployed state with all joints fastened and bonded prior to launch. The booms are ultimately deployed in a dynamic fashion by opening the cradle doors thus releasing the stored compression energy and allowing the booms to return to their original pre-launch geometry. The deployed dipole and monopole antenna configuration is illustrated along with the Mars Express spacecraft in Fig. 2. The actual antenna is a pair of 22 gage wires that run the length of the interior in all three booms.

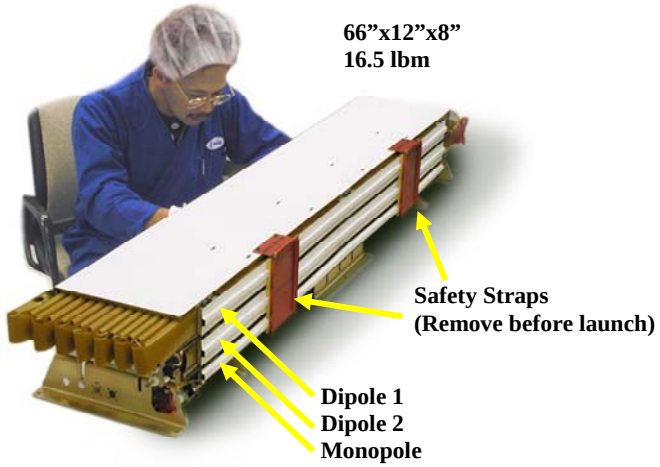

Figure 1. The stowed MARSIS antenna FFT booms and cradle prior to launch.

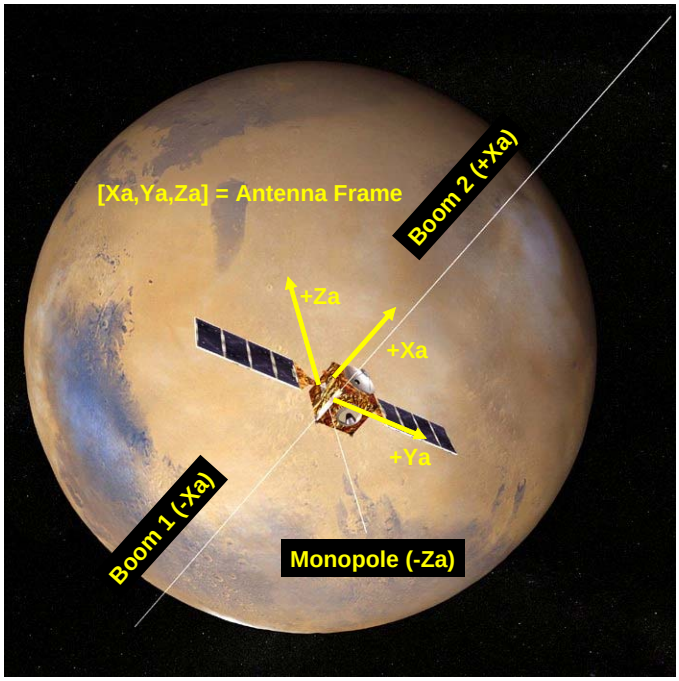

Figure 2. The three deployed MARSIS booms and reference antenna coordinate system.

This paper summarizes the resolution of an anomaly that occurred in the flight deployment of the first of a total of three MARSIS antenna booms where one of the boom hinges did not fully lock into place during the initial boom release. A short summary of some of the events following the deployment is presented as well as some of the information used to determine a course of action for the remaining two lenticular booms. Some comparisons are made between finite element modeling results and flight telemetry data in order to demonstrate the surprisingly strong understanding of the state of the partially deployed boom. Results from the accompanying

thermal analysis of the hinge are discussed and shown to support the geometry estimated from the flexible modes and spacecraft inertia measurements. The spacecraft maneuver used to warm the stalled hinge is described along with the subsequent maneuver used to mitigate the chances of a stall occurring during release of the second dipole boom. Final flight data are presented from both dipole boom deployments indicating a correctly deployed and healthy suite of antennas. The monopole deployment was detected but the final state of the boom is unknown.

II. Dipole Boom-1 Deployment

Dipole boom-1 was deployed on May 4, 2005, after which the spacecraft recovered from its post deployment attitude and was stable. However, telemetry returned from the spacecraft indicated two anomalies in the deployment: first, the deployment dynamics were outside of the Monte Carlo simulation results, and second, the spacecraft inertia and measured natural frequencies both indicated that the boom had not completely locked into place. Careful correlation between the measured spacecraft inertias and frequencies showed that hinge-10 had stalled at an angle approximately 40° from full deployment. This was a potentially serious problem as the resulting natural frequency of 0.043 Hz was inside the spacecraft's robust controller's bandwidth of 0.05 Hz.

During the deployment of dipole boom-1 the spacecraft control system was disengaged to prevent interaction of the control system with the uncertain deployment dynamics. The only data measured during the deployment were the spacecraft angular rates (sampled at 8 Hz) which were then used to infer the boom dynamics and its final state. The first 100 s of the flight measured ω_y data are plotted in Fig. 3. As indicated in Fig. 3, the primary observable frequency about the Y-axis during the deployment was at 0.144 Hz which is significantly different from the expected frequency of 0.1 Hz. In fact, there were three easily observable frequencies (and later a 4th) instead of the expected two as shown in the flexible modes test (using thruster firings) frequency results plotted in Fig. 4. Additionally, the observed damping ζ was approximately 0.6-0.8% which was well below the lower limit of 2% used in the Monte Carlo analysis; the low damping is attributed to the cold temperature which was below the glass transition temperature of the RTV used in some of the boom joints. The hinges are numbered from root to tip as shown in Fig. 5.

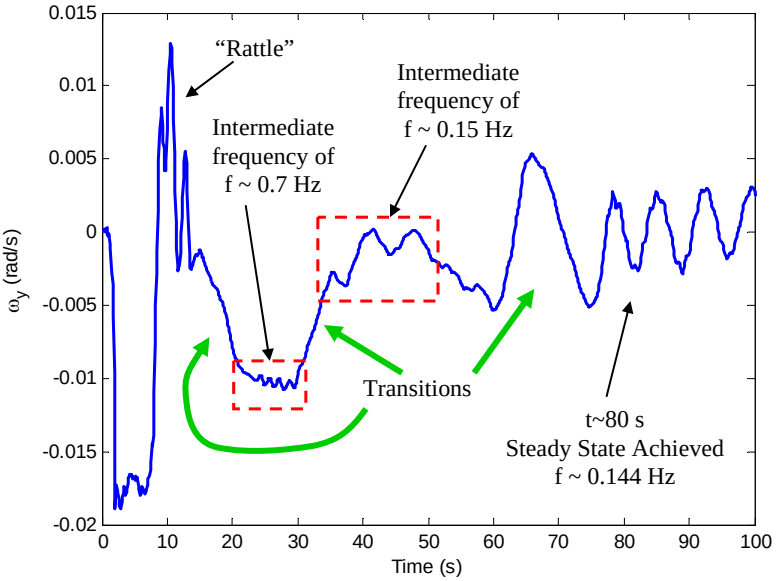

Figure 3. The spacecraft ω_y for the first 100 seconds following the dipole boom-1 deployment shows several observable intermediate frequencies that likely indicate partially locked boom segments. There were at least 4 individual hinge locking or buckling events following the initial deployment phase (including hinge-10).

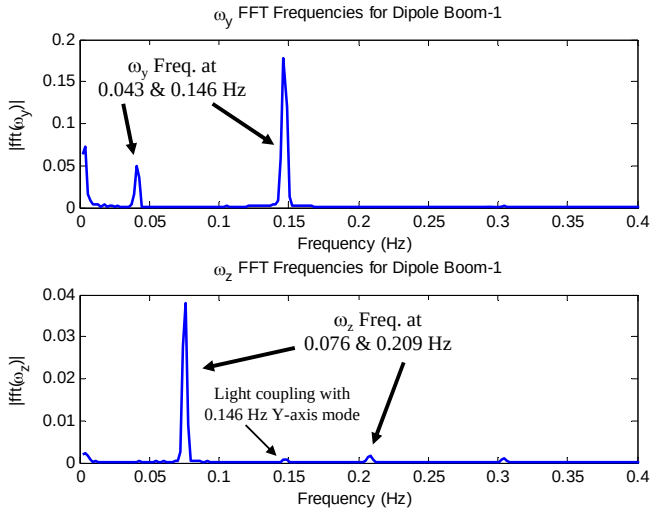

Figure 4. Dipole boom-1 measured structural frequencies following the initial deployment. These results are from the first spacecraft thruster firing test to measure the flexible modes.

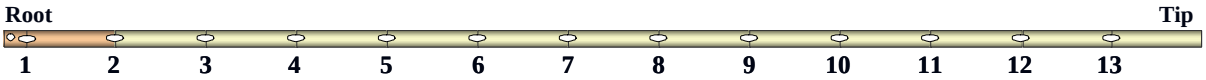

Figure 5. Dipole boom geometry with hinges numbered in increasing order from the root to the tip.

In addition to the unexpected frequencies, a careful analysis done by the flight dynamics team indicated that the expected change in spacecraft inertia was also not met. To be precise, the changes in the I_{yy} and I_{zz} terms were smaller than expected and the change in the I_{xz} term was positive rather than negative. These differences can be explained if one assumes that a single hinge location was not locked into position but was instead stalled at an angle such that the outboard portion of the boom was deflected in the positive Z-direction. The precise location could not be determined from the measured inertia changes alone but the likely candidates were identified as hinges 9, 10, and 11.

Table 1. Results from the NASTRAN study used to help determine the boom-1 state.

Hinge Number	Hinge Angle	$(\omega_y)_1$ (Hz)	$(\omega_z)_1$ (Hz)	$(\omega_y)_2$ (Hz)	$(\omega_z)_2$ (Hz)
9	65°	0.043	0.076	0.146	0.226
10	40°	0.043	0.076	0.146	0.209
11	15°	0.043	0.076	0.144	0.183
Measured	?	**0.043**	**0.076**	**0.146**	**0.209**

In an effort concurrent with the inertia measurements, the boom was modeled in NASTRAN using different assumed hinge locations and angles in an attempt to match the observed frequencies. By controlling the hinge stiffness and stall angle, it was relatively straightforward to uniquely match the three lowest observed frequencies leaving little doubt of the geometry given an a priori assumption of the location of the stalled hinge. Results from this study are summarized in Table 1. This analysis also confirmed a 4th observable frequency at 0.209 Hz which is identified in Fig. 4, although it was not used in the original model tuning. The best match to the observed frequencies, as shown in Table 1, was hinge-10 stalled at 40° from full deployment. The corresponding mode shapes from this analysis are shown in Fig. 6.

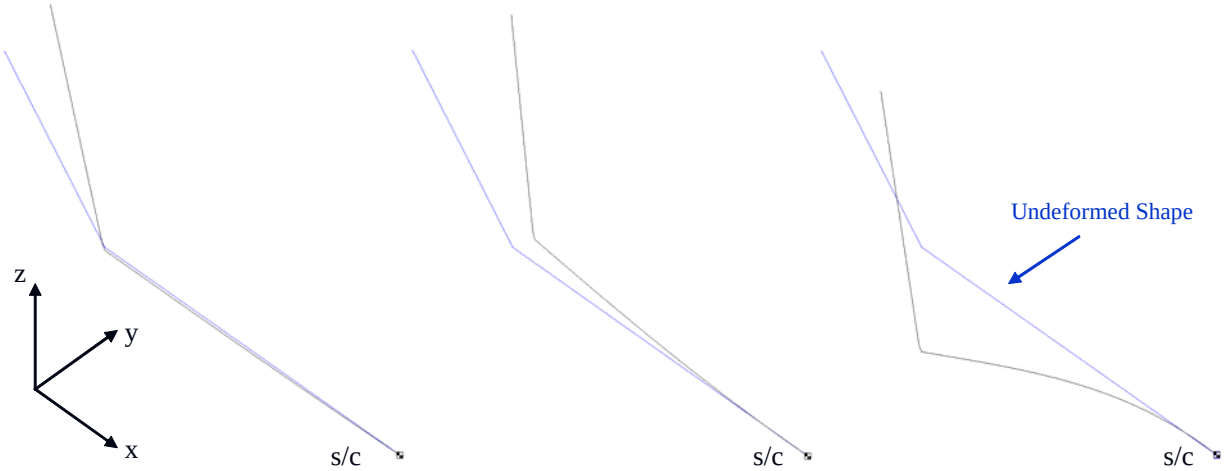

Mode 1: 0.043 Hz articulation of hinge-10 in the XZ plane.

Mode 2: 0.076 Hz swinging and rotation about the Z-axis.

Mode 3: 0.146 Hz cantilever mode in the XZ plane.

Figure 6. NASTRAN mode shapes for the partially deployed dipole boom-1 with hinge-10 stalled at 40°.

By correlating the results from the NASTRAN study with separate measurements of the spacecraft inertia, it was determined that the only case that uniquely matched both the inertia and frequency observations was that of hinge-10 stalled at an angle of 40° relative to the X-axis with the tip deflected in the +Z-direction in the X-Z plane. No other single location and geometry combination could duplicate the simultaneous match provided by this simple stalled hinge-10 model. Given this outstanding correlation to both the measured frequency and inertia properties, plans to explore multiple stalled hinge locations were abandoned.

III. Dipole-1 Anomaly Resolution

One important observation made during the hinge torque profile testing[2] was that the MARSIS hinge has a secondary stability or a stall point where the opening torque goes to zero at approximately 50° from the desired

straight geometry. This test result also matched well with the flight analysis leaving little doubt as to the boom's geometry. The average hinge torque curve developed from the component testing and used in ADAMS simulation of the deployment is shown in Fig. 7 and illustrates this behavior. This stalling phenomenon was determined to be a function of temperature and disappears as the hinge is warmed from its test temperature of -70 C to room temperature of 20 C. Careful evaluation of the flight attitude and boom geometry indicated that the hinge was in the shadow of the straight root portion of the boom as illustrated in Case-1 of Fig. 8. Thermal analysis later showed the hinge in this configuration to be very cold with portions of the hinge having temperatures below -140 C. While its threshold temperature was never measured, in every case, a stalled hinge with no change other than raising its temperature was always observed to lock into place as it warmed from its cold test temperature. The CTE expansion of the warm side and contraction of the cold side of the hinge also acted to retard its opening motion, but this was determined to be a higher order effect.

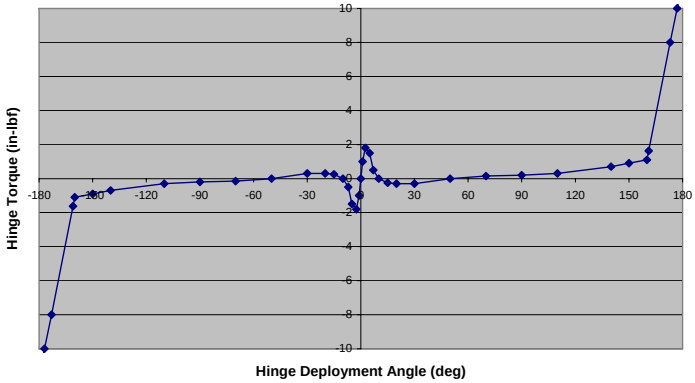

Figure 7. Average hinge deployment torque profile at -70 C. Note the onset of negative torque at ~50° that can lead to a stall condition for low rates. The artificially steep slope near 180° is intended to prevent hinge self-penetration.

After it was conclusively determined that hinge-10 was stalled at a 40° angle, and given the known temperature dependence of the stall characteristic, a possible solution was proposed that was hoped might induce the stalled hinge to deploy. Due to a bit of bad luck, the sun incidence angle on hinge-10 was initially very low and the hinge was partially in the shadow of the root section itself as shown in Case-1 of Fig. 8. While this was not the situation during the deployment, the timescale of those dynamics was to short for the sun to adequately warm the hinges and the final geometry prevented hinge-10 from warming above its deployment temperature.

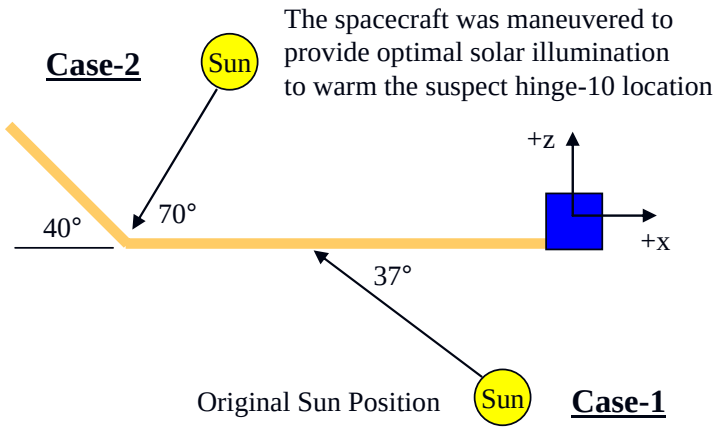

Figure 8. Case-1 shows the sun illumination of boom-1 following its initial deployment. Case-2 shows the relative sun position and illumination used to warm hinge-10 leading to its lock-out and successful deployment of boom-1.

Once the partially deployed boom-1 geometry was determined, a maneuver was performed to reorient the spacecraft and provide optimal illumination of the stalled hinge as shown in Case-2 of Fig. 8. It was hoped that the solar illumination would be sufficient to raise the temperature of the hinge above the stall threshold temperature where the secondary stability point vanishes. A more aggressive set of maneuvers involving thruster pulses to help excite the boom was also planned in the event that temperature alone was not enough. The illumination maneuver was performed on May 11, 2005, and flight data showed that, after a hold time of approximately five minutes, hinge-10 locked into place! Thermal analysis done following the boom-1 lock-out, in preparation for the boom-2 deployment, indicated that the temperature prior to the maneuver was indeed very cold as shown in Fig. 9. Following the maneuver, the temperature probably approached a steady-state value near 0 C as shown in Fig. 10.

The spacecraft measured ω_y during the Case-2 maneuver, attitude hold, and subsequent hinge-10 lock-out are shown in Fig. 11. The final measured frequencies and changes in spacecraft inertia are summarized in Table 2 and indicate that boom-1 was successfully and fully deployed.

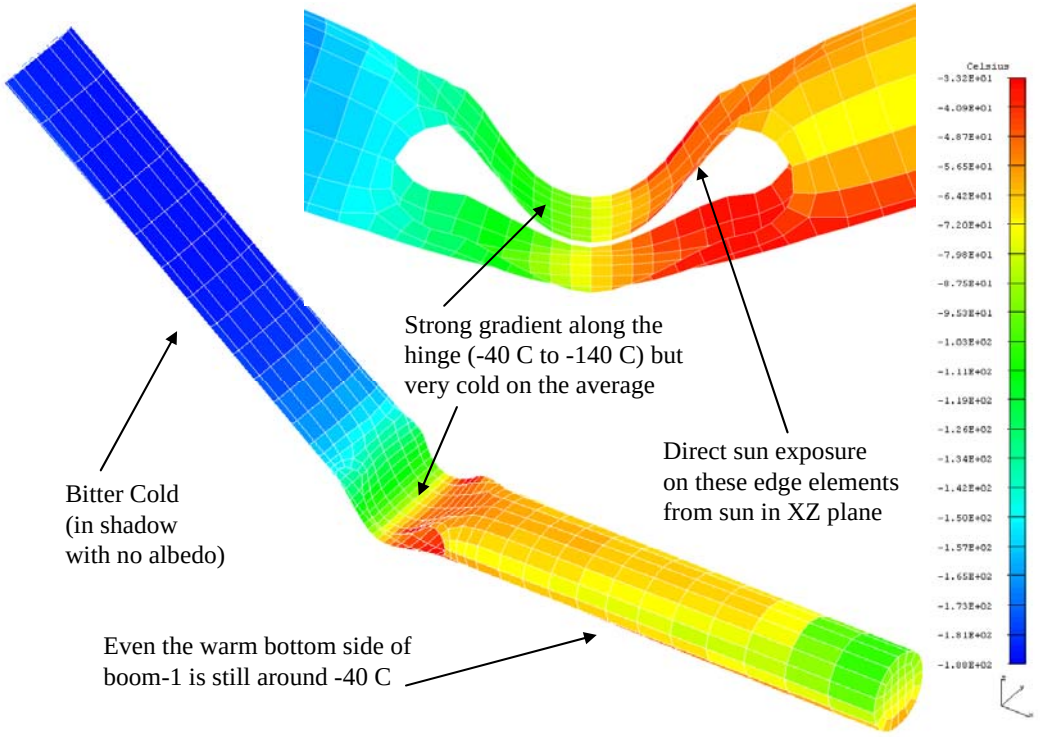

Figure 9. Radiative thermal analysis of the stalled hinge-10 during the Case-1 orientation from Fig. 8 characteristic of the spacecraft's controlled attitude following the boom-1 deployment.

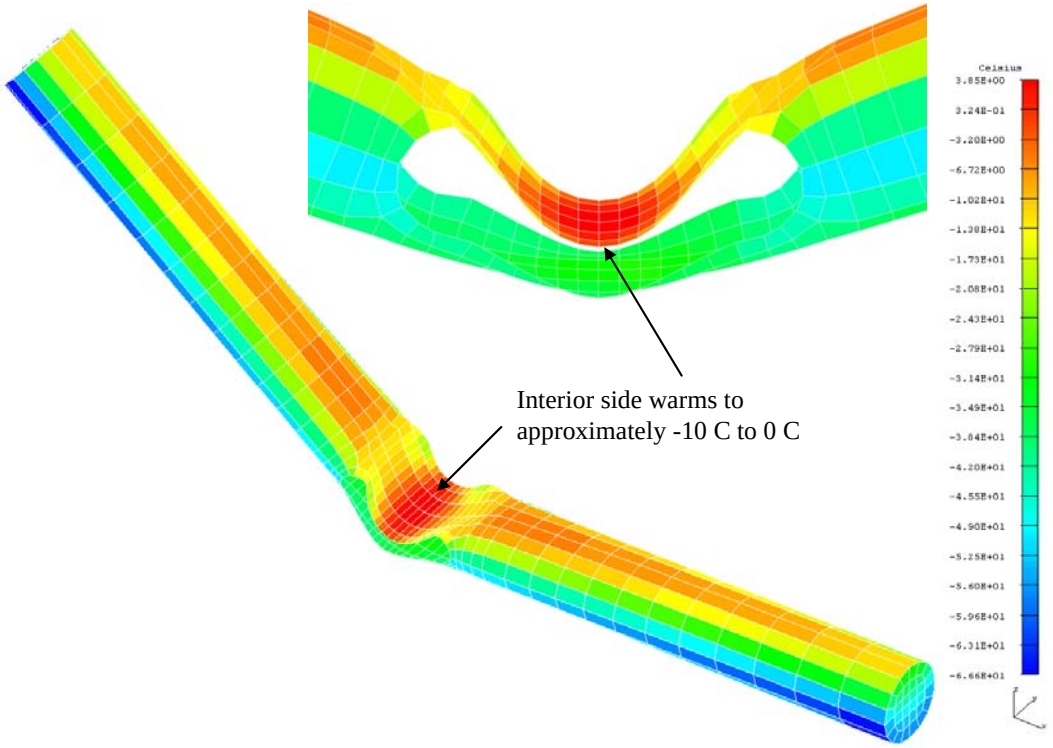

Figure 10. Radiative thermal analysis of the stalled hinge-10 during the Case-2 orientation from Fig. 8 warming maneuver that lead to the complete deployment of boom-1.

Based on experience from the boom-1 deployment, a "pirouette" spacecraft maneuver was designed that would ensure that if a similar stall occurred on the coldest (even numbered) hinges that they would be warmed in a similar fashion prior to the activation of the spacecraft controller and minimize any additional risk to the spacecraft. This maneuver, diagrammed in Fig. 12, was constrained by MEX thermal requirements to limit solar exposure of the star scanners which are mounted on the –X side of the spacecraft. The original procedure had called for orienting the spacecraft to place boom-2 in shadow prior to deployment in order to minimize its deployment energy. This maneuver was canceled in light of the temperature sensitivity of the hinges.

Table 2. Comparison of expected and measured frequencies and changes in spacecraft inertia.

	EXPECTED	AFTER INITIAL DEPLOYMENT	AFTER HINGE-10 LOCK-OUT
Change in Spacecraft Inertia:	0 -9 -5 -9 +139 0 -5 0 +139	0 -11 **+6** -11 **+132** +1 **+6** +1 **+132** *Δlxz has wrong sign* *Δlyy & Δlzz < expected*	-4 -11 **-2** -11 **+138** +1 **-2** +1 **+139**
Damping:	**3.5%**	**<1.0%**	**<1.0%**
Flexible Modes:	x None y ~0.1 Hz z ~0.1 Hz	x None **y 0.043 Hz*** **y 0.146 Hz** **z 0.076 Hz**	x None **y 0.102 Hz** **z 0.095 Hz**

**The 0.043 Hz mode was also excited by eclipse and solar array rotations.*

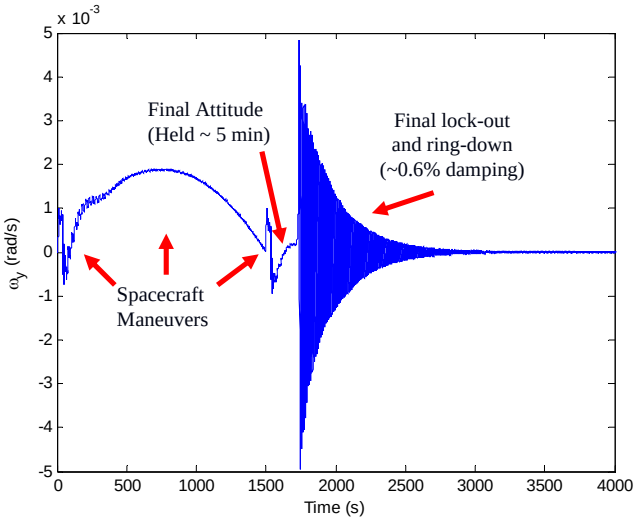

Figure 11. Measured spacecraft ω_y during the Case-2 maneuver to warm the interior of hinge-10 leading to its final lock-out and successful deployment of boom-1.

Unfortunately, it was not possible to simultaneously warm both the odd and even numbered hinges prior to deployment as they were on opposite sides of the cradle. Also, the even numbered hinges were "interior" hinges (inside the close cradle) as shown in Fig. 1, and were much more difficult to warm using solar illumination. The decision was made to warm the odd numbered hinges in order to ensure that the root hinge would lock into place. One of the most serious risks was the possibility that a hinge closer to the spacecraft could stall which would produce a low frequency mode that also had a high effective mass. A combination such as this could have potentially crippled the spacecraft's controller. To guard against a potential even (and possibly odd) numbered hinge stall, the spacecraft was given an initial spin rate of 0.1°/s prior to the deployment command with the reaction control wheels essentially spun down and uncontrolled throughout. The full maneuver was performed over a 30 minute period.

Good fortune shone on the deployment of dipole boom-2 on June 14, which was uneventful and produced exactly the expected resonant frequencies and changes to the spacecraft inertia. The resulting flight ω_y data result is plotted in Fig. 13 with some

Table 3. Comparison between flight measured flexible mode frequencies and NASTRAN model results.

Mode Number	Predicted Freq. (Hz)	Measured Freq. (Hz)	Difference (Hz)	Sensing x-axis	Sensing y-axis	Sensing z-axis
1	0.086	0.085*	n/a		SYMM	
2	0.089					SYMM
3	0.100	0.100	0			ASYMM
4	0.115	0.115	0		ASYMM	
5	0.355	-	-	ASYMM		
6	0.357	-	-		ASYMM	
7	0.541	-	-		SYMM	
8	0.547	0.54	-0.007		ASYMM	
9	0.558	-	-			SYMM
10	0.560	0.56	0			ASYMM

*Cross-talk sensing through y-axis and z-axis

annotation. As anticipated, the deployment of boom-2 excited the flexible modes of boom-1 which are then present throughout the collected data; hence, it is very difficult to make any meaningful conclusions regarding the boom-2 dynamics.

The 7 m monopole boom was deployed on June 17, also without incident. Unfortunately, due to its very low mass and inertia, the final state of the monopole is currently uncertain and may never be known (the radar also cannot be used to check its geometry) but it was determined not to present a risk to the spacecraft regardless of its final state.

A comparison between the flight measured modal frequencies and the NASTRAN modeled frequencies for the final deployed configuration (illustrated in Fig. 2) is given in Table 3. The boom properties in the NASTRAN model were tuned to match the deployed frequencies measured after dipole boom-1 locked into place. Note that the lowest frequency drops from 0.095 Hz with only boom-1 deployed to 0.085 Hz with all three booms deployed. The reason for this is that a single boom acts to rotate the spacecraft at its cantilevered root while the symmetric dipole booms act to translate the spacecraft when the booms deform symmetrically. Therefore, the fully deployed state is closer to a fixed boundary condition and has a corresponding lower frequency.

The correlation to flight data is excellent with only tiny discrepancies in frequency. Modes 1 and 2 are symmetric with respect to the Y and Z-axes and couple with each other about the X-axis. Nevertheless, a single frequency peak was still detectable due to their offset location with respect to the spacecraft cg which resulted in rotation about the X-axis; e.g., if the spacecraft translates along the Z-axis, because the booms lie on the negative Y-axis, the motion will generate a moment about the X-axis. Similarly, a spacecraft motion along the Y-axis will also generate a moment about the X-axis. Hence, the fundamental symmetric modes are coupled and are not easily visible on the Y or Z-axes. Note that the pre-launch fixed-base predicted frequencies for modes 1 and 2 were 0.078 Hz and 0.081 Hz, which are very close to the measured flight frequencies in Table 3. All of the other asymmetric modes were detectable up to the 10th flexible mode with the exception of the monopole modes which had too little effective mass to be seen.

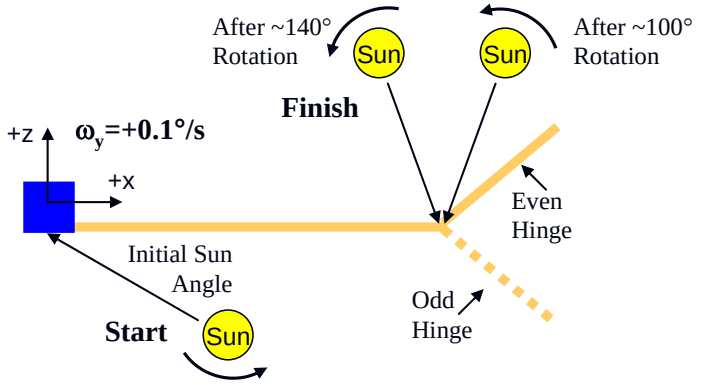

Figure 12. Spacecraft slew maneuver used during the dipole boom-2 deployment. The maneuver was designed with a primary goal to illuminate the interior of an even numbered hinge should one stall. Thermal analysis also showed that perpendicular illumination of the back of an odd numbered hinge resulted in moderate warming with a significant chance that a stalled odd numbered hinge might be unfrozen as well.

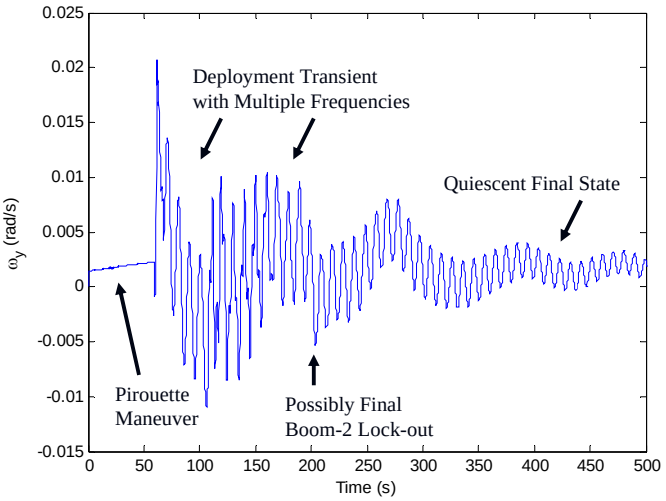

Figure 13. Measured spacecraft ω_y during the dipole boom-2 deployment. Note that boom-1 is excited at the onset and rings throughout the boom-2 deployment.

IV. Concluding Remarks

First and foremost, the authors strongly recommend that the reader not take lenticular (carpenter tape) structures for granted. The mechanisms and sensitivities of these joints are complex and the use of multiple hinges greatly amplifies the modeling challenges. Material selection and construction can have subtle effects on the hinge behavior which, depending on the materials chosen, can also be strongly dependent on the in-situ temperature. Ideally the

hinges should have a positive torque margin throughout their range of motion. These hinge characteristics should be tested to verify their torque characteristics. The tests should closely approximate flight conditions especially temperature, aging, and thermal cycling effects such as from aerobraking, whenever possible.

The total stowed energy should be optimized (neither to high nor too low) to control the dynamics in the deployment. The tube compression energy should be low enough to prevent the back-buckling phenomenon but, simultaneously, the hinge energy needs to be high enough to produce positive torque throughout the hinge range of motion. These types of lenticular booms are extremely lightweight and, once in their proper deployed state, are very easily modeled and accounted for on the spacecraft. Unfortunately, it is not possible to perform a meaningful full system test on the ground so an accurate component model of the boom is extremely important.

Acknowledgments

The authors would like to acknowledge the hard work and thorough analysis of the ESA and EADS Astrium engineering and flight team. The odyssey of MARSIS was indeed a job well done. The research described in this paper was carried out at NGST Astro Aerospace (Contract No. 1263269) and at the Jet Propulsion Laboratory, California Institute of Technology, under a contract with the National Aeronautics and Space Administration.

References

[1]Marks, G.W., Reilly, M.T., and Huff, R.L., "The Lightweight Deployable Antenna for the MARSIS Experiment on the Mars Express Spacecraft," 36th Aerospace Mechanisms Symposium, Glenn Research Center, May 14-17, 2002.

[2]Mobrem, M., and Adams, D. S., "Analysis of the Lenticular Jointed MARSIS Antenna Deployment," 47th AIAA Structures, Structural Dynamics, and Materials Conference, May 1-4, 2006, Newport, Rhode Island, AIAA-2006-1683.

[3]Adams, D. S., Mobrem, M., and Sabahi, D., "MARSIS Antenna Deployment Testing and Analysis," Spacecraft and Launch Vehicle Dynamic Environments Workshop, June 21-23, 2005, Aerospace Corporation, El Segundo, California.